Journal of Climate Change
ISSN 2395-7611 Volume 11 (2025) No. 4. pp. 534–554

https://doi.org/10.70917/jcc-2025-035
Article

Towards Climate-Resilient Data Center Cooling: Experimental Study of Water Conservation Technologies

Lu Wang, Liang Chen and Zhen Li *

Key Laboratory for Thermal Science and Power Engineering of Ministry of Education, Department of Engineering Mechanics, Tsinghua University, Beijing 100084, China
* Correspondence author: lizh@tsinghua.edu.cn

Abstract: The rapid expansion of data centers, driven by the proliferation of 5G and cloud technologies, has intensified environmental concerns, particularly related to water consumption and energy use. Data centers consume billions of liters of water daily for cooling, with wet cooling towers accounting for the majority of this usage. Despite various efforts, effective strategies to reduce water consumption in these systems remain limited. This study proposes the use of hygroscopic solutions as alternative cooling media in wet cooling towers to address this challenge. An experimental system was developed to evaluate this technology's performance. The results demonstrate a significant reduction in water consumption of up to 84.72% while maintaining comparable thermal performance to traditional systems. For data center operators, especially those in water-stressed regions, this technology offers a viable path to drastically lower operational water costs and reduce environmental impact, supporting compliance with increasingly stringent sustainability regulations. The water-saving mechanisms are further explored through an analysis of the interactions between the hygroscopic solution and moist air, utilizing physical properties and enthalpy-humidity charts. This research contributes to sustainable cooling strategies essential for adapting to water stress and environmental demands in an era of accelerating technological growth.

Keywords: Water saving; Wet cooling tower; Hygroscopic solutions; Data center; Climate resilience

1. Introduction

In the rapidly evolving domain of information technology (IT), the expansion of data processing demands has led to an exponential increase in data center proliferation (Masanet et al., 2020, Abbas et al., 2021, Han et al., 2021). Recent data analyses show that the global data center industry reached a scale of $130.8 billion in 2022, with its power consumption reaching 460 TWh, accounting for 2% of the global total electricity demand (Du et al., 2024, Refrigeration, 2023). This surge in energy demand is compounded by the challenges of cooling these facilities, where overheating has become a critical issue. Cooling systems, in particular, have emerged as major energy consumers, accounting for approximately 40% of a data center's total energy use, making low-energy refrigeration an urgent research priority. (Xu et al., 2023, Li et al., 2023, Ni and Bai, 2017, Silva-Llanca et al., 2023, Cheung and Wang, 2019, Kutlu et al., 2025, Suman et al., 2025).

Effective thermal management in large-scale data centers typically involves the use of cooling towers, which are divided into wet and dry systems based on their operational mechanisms. These towers play a crucial role in dissipating heat from the coolant, which cycles through heat exchangers to ensure the continuous operation of data center cooling (He et al., 2022). Dry cooling towers remove heat by passing coolant through cooling fins, coupled with forced air cooling to the environment. However, they often suffer from suboptimal heat exchange efficiency due to the multiple contact interfaces, also lead to increased operational costs in cold climates because of the need for frost protection measures. Conversely, wet cooling towers utilize direct convection and evaporation of coolant—typically water—for heat removal, facilitated by the direct interaction between the coolant and air, achieving high heat dissipation performance. As such, wet cooling towers are favored in large-scale data centers, with a majority

employing counterflow designs (Akbarpour Ghazani et al., 2017, Asvapoositkul and Kuansathan, 2014) for enhanced cooling efficiency. Yet, despite their superior efficiency and cost-effectiveness, the significant water consumption of wet cooling towers raises substantial sustainability concerns, with reports indicating that 65 %-75 % of a data center's total water use is attributed to these systems (El Marazgioui and El Fadar, 2022, Cuce, 2025). Enhancing the water usage efficiency of wet cooling towers is thus imperative for improving the sustainability of data center operations.

Existing investigations into wet cooling towers have largely been directed towards augmenting heat transfer efficiencies, with minimal emphasis on addressing water consumption challenges (Mirabdolah Lavasani et al., 2014, Xi et al., 2023, Zhao et al., 2023, Zhang et al., 2024). The limited research aimed at curbing water use has mainly revolved around operational adjustments—regulating water flow rates, modifying air conditions, and refining the design of internal components (Deng and Sun, 2024, García Cutillas et al., 2017, Liu et al., 2023, Taghian Dehaghani and Ahmadikia, 2017, Yuan et al., 2020). However, such measures generally yield only marginal reductions in water usage and may encounter practical implementation hurdles due to manufacturing constraints. In contrast, replacing coolant water in wet cooling towers with alternative fluids presents a straightforward and potentially more effective solution (Imani-Mofrad et al., 2018, Javadpour et al., 2021). This approach preserves the cooling system's structure, eliminating the need for extensive modifications. However, relevant experimental studies remain limited, and there is a lack of understanding of the underlying mechanisms, hindering the identification of optimal water-saving coolants and resulting in relatively low water-saving efficiency. The few existing studies have not achieved substantial water savings. For example, Askari et al. (Askari et al., 2016) found that incorporating multi-walled carbon nanotubes and nanoporous graphene nanofluids into coolant water improves heat transfer efficiency but only reduces water consumption by 10-19%. Other studies have explored using saline water as an alternative coolant to conserve water, but even with high concentrations of saline water, the potential for significant water savings remains limited (Qi et al., 2016, Qu et al., 2024, Yan et al., 2024, Shublaq and Sleiti, 2020, Sharqawy et al., 2011). Thus, it is still essential to explore alternative, efficient circulating media for cooling towers and investigate their water-saving mechanisms to enhance performance.

This study introduces a novel water-saving counterflow wet cooling tower that employs hygroscopic solutions as an economical, efficient, and non-toxic alternative to traditional water. The heat and mass transfer performance of hygroscopic salt solutions, including $CaCl_2 \cdot H_2O$, $LiBr \cdot H_2O$, and $LiCl \cdot H_2O$, is analyzed, offering practical guidance for solution selection in real-world applications. A mechanically ventilated counterflow cooling tower experimental system is designed and implemented to evaluate the performance of hygroscopic solutions comprehensively. Experimental results demonstrate that hygroscopic salt solutions can reduce water consumption by up to 84.72%, the highest reduction reported in the literature, while maintaining comparable heat exchange efficiency (Wan et al., 2020, Sadafi et al., 2015). Furthermore, the water-saving mechanisms of the system are explored. These findings offer valuable insights into reducing water consumption in data center cooling systems and underscore the potential for integrating sustainable practices into environmentally-conscious data centers.

2. Evaluation of cooling tower performance parameters

2.1. Structure and operation of counterflow wet cooling towers

Figure 1 presents a schematic of a counterflow wet cooling tower, highlighting its structural components. The operation begins with the cooling medium—water or a solution—being fed into the tower through the top inlet. This medium is evenly spread across the tower's cross-section via a tubular distribution system, then dispersed over the fill material using nozzles. This setup ensures direct contact between the cooling medium and the air, flowing in the opposite direction, thus facilitating efficient heat exchange. The air enters the tower through an intake at the bottom, moving upward counter to the cooling medium, absorbing heat, and then exiting as warmed air through the top fan system. The cooled medium collects in the sump at the tower's base, ready for recirculation. The process is characterized by opposing flows of air and the cooling medium, enhancing heat transfer efficiency.

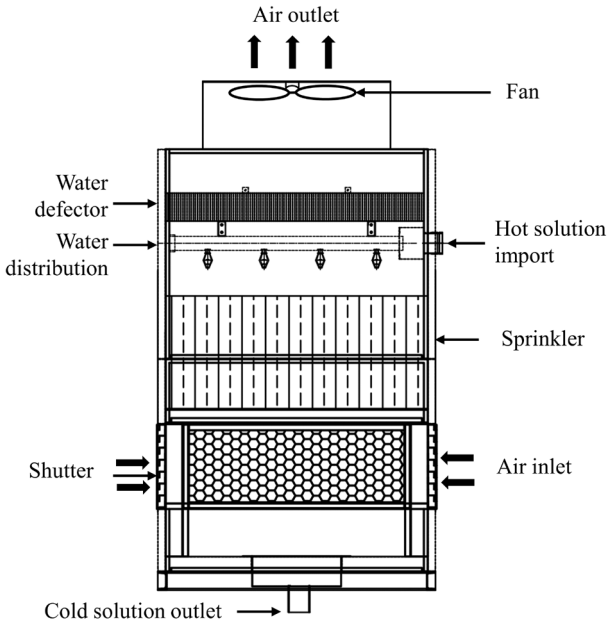

Figure 1. Schematic diagram of a wet cooling tower with a counterflow packing tower configuration.

2.2. Cooling tower modeling and parameter analysis

This subsection outlines key parameters and thermodynamic models essential for assessing cooling tower efficiency. In wet cooling towers, heat is transferred from the hot cooling medium to the air and then released into the atmosphere. Radiative heat loss within the tower is minimal and, therefore, omitted from this analysis. The primary mechanisms of heat transfer are conduction and evaporation. This process simultaneously involves the cooling and mass reduction of water, as well as the heating and humidification of the air.

The distribution of the cooling medium and air is almost uniform across any horizontal section, allowing the coolant-air interaction within the tower to be modeled as a one-dimensional process, as shown in Figure 2. Furthermore, although the vapor's partial pressure may vary within the tower, its impact on the overall pressure is insignificant. This allows for the assumption of a constant atmospheric pressure throughout the cooling tower.

Figure 2(b) presents a schematic representation of the equivalent physical model based on the two-film theory. A thin layer of air exists at the surface of the liquid phase, which is assumed to be in phase equilibrium with the bulk liquid. According to the equivalent physical model of the two-film theory (Whitman, 1962), heat and mass transfer occur between the surrounding air and an extremely thin layer of equivalent humid air at the surface of the cooling medium (water or solution). This equivalent humid air represents the air that is in equilibrium with the liquid phase.

Heat and mass exchange are facilitated by this equilibrium air layer. When the water temperature is higher than the air temperature, heat transfers from the liquid to the air. Similarly, water vapor moves from the liquid film to the air when the film's vapor pressure is higher. Conversely, water vapor moves from the air to the film when the air's vapor pressure is higher. During evaporation, water vapor lost from the film is replenished by active movement of water molecules from the liquid surface. In condensation, excess vapor in the film returns to the liquid, keeping the film saturated. Heat transfer is driven by the temperature difference between the air and liquid, while mass transfer is driven by the vapor pressure difference. The efficiency of heat and mass transfer depends on these differences.

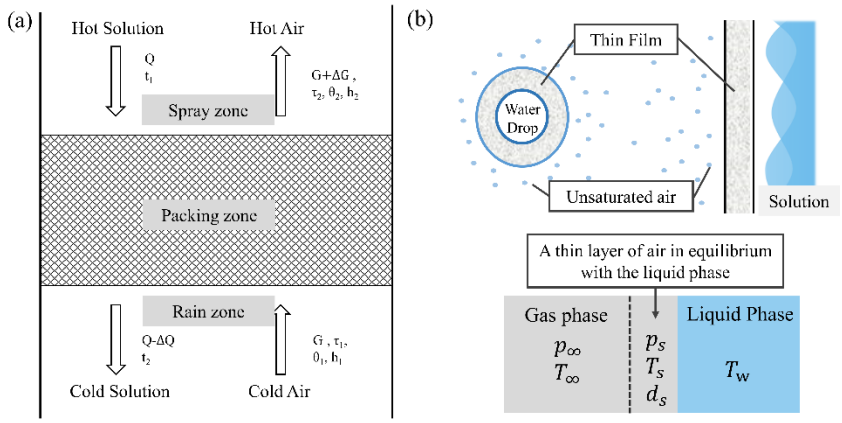

Figure 2. **(a)** Schematic diagram of the thermal property calculation for the wet cooling tower; **(b)** Equivalent physical model of double membrane theory.

The cooling medium descends from above, entering with a flow rate of Q (kg/h) and temperature t_1 (°C), and exits with a reduced flow rate of Q-ΔQ (kg/h, ΔQ representing the volume of evaporated coolant) and temperature t_2 (°C). The dry air passing through the tower is quantified by a flow rate of G (kg/h), entering with dry-bulb temperature θ_1 and wet-bulb temperature τ_1, and exiting with temperatures θ_2 and τ_2, respectively. Despite fluctuations in the vapor's partial pressure within the tower, its relative contribution to the total pressure remains minimal. Consequently, the atmospheric pressure can be considered constant within the cooling tower.

Thus, the mathematical expressions of the key parameters within the cooling tower can be outlined as follows. The cooling medium enters from above, with a flow rate of Q and temperature t_1, and exits with temperature t_2 and a diminished flow rate of, Q-ΔQ where ΔQ symbolizes the evaporated coolant volume. The airflow through the tower, quantified by a mass flow rate G, enters with a dry-bulb temperature θ_1 and wet-bulb temperature τ_1, and exits at temperatures θ_2 and τ_2, respectively. The flow rate G is determined by the product of the cross-sectional area A of the tower's air inlet and the measured wind speed u. The air-to-liquid ratio λ, a critical performance indicator, is calculated as the ratio of air volume flow rate G_{vol} to the cooling medium's mass flow rate M (Eq. 1):

$$\lambda = \frac{G_{\mathrm{vol}}}{M} = \frac{Au}{M}. \tag{1}$$

The temperature difference of the cooling medium is equal to the difference of the inlet temperature T_1 and the outlet temperature T_2:

$$\Delta T = T_1 - T_2. \tag{2}$$

The thermal efficiency (η) of the cooling tower, indicative of its thermal performance, is defined as the ratio of the cooling tower's temperature range to the temperature difference between the incoming coolant and the inlet air's wet-bulb temperature,

$$\eta = (T_1 - T_2)/(T_1 - T_{\mathrm{wb}}). \tag{3}$$

Here, T_{wb} represents the inlet air's wet-bulb temperature, setting the cooling limit for circulating water in a wet cooling tower. The total heat transfer rate, Q_{h}, is the product of the coolant's mass flow rate and its enthalpy change,

$$Q_{\mathrm{h}} = M \cdot (h_2 - h_1). \tag{4}$$

Another pivotal measure, the cooling number N, reflects the tower's cooling capacity. It is derived through the enthalpy difference method (EDM) (Merkel, 1925, El-Dessouky et al., 1997, Khamis Mansour, 2017), which is a proven and widely used approach for thermodynamic analysis in cooling towers. Since the driving force of total heat exchange between solution and air is enthalpy difference. N is defined as

$$N = \frac{c}{K}\int_{t_1}^{t_2} \frac{dt}{i'' - i}, \tag{5}$$

where c is the specific heat capacity of the coolant, K is a coefficient related to evaporated coolant volume, i'' is the enthalpy of the saturated air above the coolant surface, and i is the enthalpy of moist air. A larger N value signifies greater heat dissipation needs, implying a larger capacity for the water sprinkling device. In this work, the Simpson's integration is used to calculate the cooling number numerically (Hill et al., 2013).

3. Experimental system and method

3.1. Experimental system

This study developed a mechanically ventilated counterflow wet cooling tower experimental system for experimental analysis. Figure 3 presents the schematic representation of the experimental configuration of the cooling tower. The system encompasses an integrated setup comprising external circulation, internal hot fluid circulation, and a comprehensive data acquisition system.

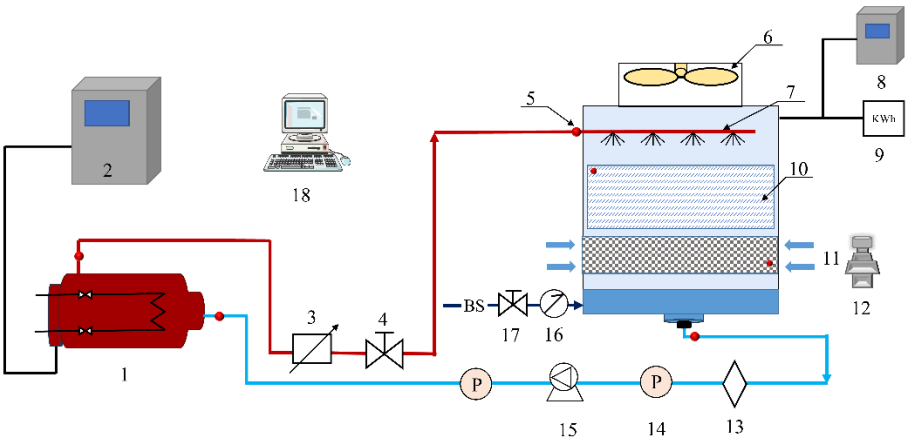

1) Pipe heater 2) Control cabinet 3) Electromagnetic flowmeter 4) Control valve 5) Thermocouple 6) Variable frequency fan 7) Water distribution device 8) Variable frequency drive 9) Power meter 10) Packing device 11) Air inlet 12) Portable weather station 13) Filter 14) Pressure gauge 15) Variable frequency water pump 16) Water meter 17) Make-up water valve 18) Data acquisition instrument

Figure 3. Schematic diagram of the experimental system.

As illustrated in Figure 4, the experimental apparatus was placed outdoors to enhance the efficacy of the testing process. The experimental protocol for the cooling tower is delineated as follows. The initial step involves filling the cooling tower and its associated circulation pipes with an adequate amount of coolant. Subsequent temperature regulation and adjustment of the inflowing water are executed via a pipe heater and a control cabinet. This process utilizes a Proportional-Integral-Derivative (PID) temperature control strategy, coupled with a variable frequency drive to activate the airflow mechanism.

Air is directed to move sequentially through the packing area, which is equipped with cross-lattice type packing, then through the spray device, and finally past the fan to the outlet. This airflow follows an upward trajectory from the inlet at the base of the cooling tower. Simultaneously, the circulating medium is driven downwards by the circulating pump, facilitating a heat exchange with the air within the packing area. To minimize thermal losses, insulation is applied to the circulation pipes. Upon achieving system stability, measurements are systematically recorded.

Experiments were conducted varying the inlet temperature of the cooling tower and the mass flow rate of the circulating medium. For each operational condition, we measured parameters such as the inlet and outlet temperatures of both fluid and air, humidity, wind speed, circulating medium's mass flow rate, and water consumption, etc. Thermocouples were installed on the conduits of the circulating fluid to record temperature readings. Specifically, thermocouples were installed at both the inlet and outlet of the cooling tower, as well as at the inlet and outlet of the pipe heater. All temperature measurement points were connected to a centralized control system, continuously monitored by a computer for sampling.

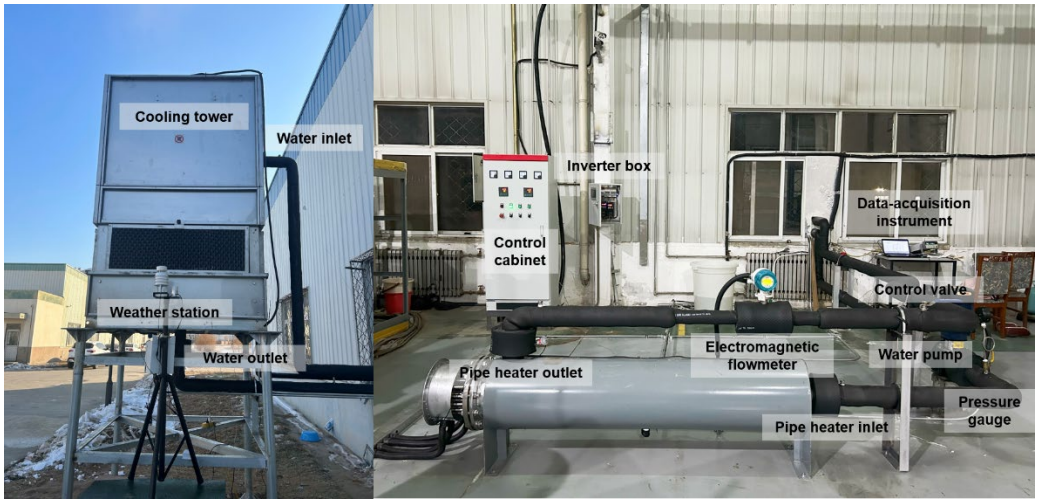

Figure 4. Photograph of the wet cooling tower test system.

The air's dry and wet-bulb temperatures, as well as its relative humidity, were precisely measured in real-time using a hygrothermograph and a portable weather station. An electromagnetic flowmeter, located at the outlet of the pipe heater, enabled direct data retrieval from its display. Air velocities at the cooling tower's entry and exit were assessed using a wireless universal anemometer and a portable weather station, which provided readings of wind speed, temperature, and relative humidity.

Upon determining the required variables, we used the psychrometric chart to identify unknown variables like enthalpy, specific humidity, dew point temperature, and vapor pressure. These values were then utilized to calculate performance parameters, including cooling water range, cooling tower thermal efficiency, and cooling number, etc. Through thermodynamic analysis of various operational states, the actual cooling capacity of the cooling tower was ascertained, offering an assessment of the tower's cooling efficiency.

3.2. Uncertainty analysis

To ensure the accuracy and reliability of the experimental results, uncertainty analysis was conducted for all key measured parameters. Table 1 summarizes the instruments used, their respective measurement ranges, and uncertainties. The uncertainty of each parameter was considered based on the specifications of the measurement instruments. Temperature measurements were conducted using a Type T thermocouple. The T-Type thermocouple was employed to monitor temperature distribution within the fill and at the inlet and outlet of the cooling tower. All T-type thermocouples were calibrated using a standard glass mercury thermometer and a high-precision thermostatic water bath. The measurement uncertainty of the T-type thermocouples was within ± 0.5 °C.

The hygrothermograph provided additional inlet and outlet air temperature and humidity measurements, with a relative humidity uncertainty of 0.1% and a temperature uncertainty of ± 0.1 °C. The portable weather station was used to monitor multiple ambient parameters. It recorded wind speed with an uncertainty of ±0.1 m/s, relative humidity with an uncertainty of ±3% RH, and air temperature with an uncertainty of ±0.3 °C. Additionally, it provided measurements of atmospheric pressure and solar radiation, with uncertainties of ±0.15 kPa and ±3%, respectively. These parameters were essential for capturing environmental conditions and assessing the influence of external factors on the heat and mass transfer process.

Table 1. Experimental Instruments and Measurement Parameters.

Instrument	Model	Measurement Range	Uncertainty	Measurement Parameters
Thermocouple	Type T	-200℃-350℃	±0.5 °C	Temperature distribution, Inlet/outlet temperature
Portable weather station	QZQXZ-BXCS-4G-1	wind speed: 0 m/s-60 m/s; relative humidity: 0% -99%;	wind speed: ± 0.1m/s; relative humidity: ± 3% RH;	Ambient air velocity, temperature, humidity, pressure

		temperature: -40℃-120℃; atmospheric pressure: 0-120 KPa	temperature: ± 0.3℃; atmospheric pressure: ± 0.15kPa	
Hygrothermograph	WSZY-1	relative humidity: 0% -100%; temperature: -40℃-100℃	relative humidity:0.1%RH; temperature: ±0.1℃	Inlet and outlet air temperature/humidity
Electromagnetic flowmeter	GC230	2.3-45.2 m^3/h	± 0.5%	Circulating medium flow rate
Water meter	LXS-15	0-99999.9999 m^3	± 2%	Water consumption
Pressure gauge	Y-100	0-1.6 MPa	± 5%	Pipe pressure
Density meter	—	1.200-1.500 g/cm^3	± 0.25%	Solution density
Wireless anemometer	WWFWY-1	0.05 m/s - 30 m/s	5% ± 0.05m/s	Wind speed

The flow rate of the circulating medium was measured using an electromagnetic flowmeter, which has a measurement uncertainty of ±0.5%. Accurate flow measurement was essential for determining the convective heat transfer rate. Meanwhile, total water consumption was tracked using a mechanical water meter, with an uncertainty of ±2%. System pressure within the pipelines was recorded using a pressure gauge, presenting an uncertainty of ±5%. The density of the circulating solution was monitored using a density meter with a measurement range of 1.200~1.500 g/cm³ and an uncertainty of ±0.25%.

According to the error propagation theory, for a derived parameter $z = f(x_1, x_2, \dots, x_n)$, where each independent variable x_i, has a small measurement error Δx_i, the relative uncertainty of z can be expressed as:

$$\frac{\Delta z}{z} = \sqrt{\sum_{i=1}^{n} \left(\frac{\partial lnz}{\partial x_i} \Delta x_i\right)^2}. \tag{6}$$

In this study, the following derived metrics are used in performance evaluation: the temperature difference ΔT, cooling efficiency η, heat transfer rate Q and cooling number N. Their uncertainties are obtained from first-order error propagation using Eq. 6.

The uncertainty of the ΔT was calculated using Equation (6), which combines the uncertainties of the two thermocouples in quadrature, yielding a combined standard uncertainty of 0.71 °C. The uncertainty of η is driven by the inlet and outlet water temperatures and the inlet air wet-bulb temperature. It increases when the cooling approach becomes small. Under the operating conditions of this study, the estimated uncertainty of η is approximately ±10%. The uncertainty in the λ originates from the inlet area, air velocity, and coolant mass flow measurements. The mass flow uncertainty (0.56%) comes from the flowmeter (±0.5%) and density meter (±0.25%), while the contribution from the tightly-toleranced inlet area is negligible. The relative uncertainty of λ is estimated to be between ±5% and ±7%.

The uncertainty of Q, which is governed by the uncertainties in mass flow and enthalpy change, is typically dominated by the uncertainty of ΔT when the constant heat-capacity approximation is used, as the contribution from c_p is negligible over narrow temperature spans. The relative uncertainty of Q remains within ±12%. The cooling number N is computed numerically using Simpson's rule. Its associated uncertainty is obtained by perturbing the psychrometric inputs within their instrument specifications. The dominant contributors to this uncertainty are the air temperature, relative humidity, and the water temperature, which is used to evaluate the saturated-air properties. In contrast, the effect of pressure uncertainty (±0.15 kPa) is minor. The relative uncertainty of N is estimated to range from ±6% to ±13%.

The experimental setups featured cooling tower inlet flow rates of 15 to 30 m³/h, inlet temperatures between 14 to 22 °C, and λ ranging from 0.4 to 1.0. To ensure uniform environmental conditions, the experiment was conducted during periods of stable ambient temperature and humidity, with air inlet temperature differences kept below 3°C and relative humidity changes less than 5% over an extended period. Considering the extended measurement period needed to assess water consumption, exceeding a single day, experiments were scheduled during periods with consistent environmental temperatures and humidity levels. Data collection and processing were performed under the cooling tower's stable operating conditions throughout the experiment. The experiment included intervals for monitoring the

solution's density to ensure consistency with the initial settings. The same experimental condition was carried out at least twice to ensure repeatability. The variance between runs for key performance metrics, such as outlet water temperature and thermal efficiency, was observed to be less than 3% under identical operating conditions, confirming the high consistency of the results presented.

4. Results and discussions

4.1. Heat and mass transfer analysis of solution-based cooling towers

This study analyzes the heat and mass transfer processes of common hygroscopic salt solutions, including $CaCl_2·H_2O$, $LiBr·H_2O$, and $LiCl·H_2O$, within wet cooling towers. In the analysis of heat and mass transfer between the solution and air, the concept of equivalent humidity ratio ω_e is introduced, which is determined by the vapor pressure at the solution's surface. When the hygroscopic solution is in equilibrium with moist air, their temperatures and water vapor partial pressures are identical. Under equilibrium conditions, the surface vapor pressure of the solution approximately equals the water vapor partial pressure. The equivalent humidity ratio of the solution corresponds to the humidity ratio of the air in equilibrium with the solution, as given by Eq. 7:

$$\omega_e = 0.622 \frac{p_s}{p_b - p_s}, \tag{7}$$

where ω_e is the equivalent humidity ratio of the solution (kg/kg of dry air), p_b is the atmospheric pressure, and p_s is the surface vapor pressure of the solution.

On the enthalpy-humidity chart, the isoconcentration lines of the solution align closely with the lines of constant relative humidity for moist air. This indicates that the vapor pressure equations for different solutions share similar forms and can be described using analogous mathematical models. This study adopts the model proposed by Conde (Conde, 2004) to calculate the surface vapor pressure and density of $CaCl_2·H_2O$ and $LiCl·H_2O$ solutions, Siddig-Mohammed et al.'s (Siddig-Mohammed et al., 1983) empirical relations to determine the specific enthalpy of $CaCl_2·H_2O$, Chaudhari et al.'s (Chaudhari and Patil, 2002) thermodynamic method for $LiCl·H_2O$ enthalpy, and Patek et al.'s (Pátek and Klomfar, 2006) model for the surface vapor pressure, density, and specific enthalpy of $LiBr·H_2O$ solutions. Using these models, the equivalent humidity ratios for various solutions are calculated, and their states can be represented on the enthalpy-humidity chart corresponding to the equilibrium moist air state. Figure 5 illustrates the positions of $CaCl_2·H_2O$, $LiCl·H_2O$, and $LiBr·H_2O$ solutions on the enthalpy-humidity chart. The isoconcentration lines of the solutions approximately coincide with the constant relative humidity lines of moist air. It is evident from the chart that solutions with lower temperatures and higher concentrations exhibit lower equivalent humidity ratios. When using hygroscopic solutions with the same temperature and equivalent humidity ratio, similar cooling effects can be achieved.

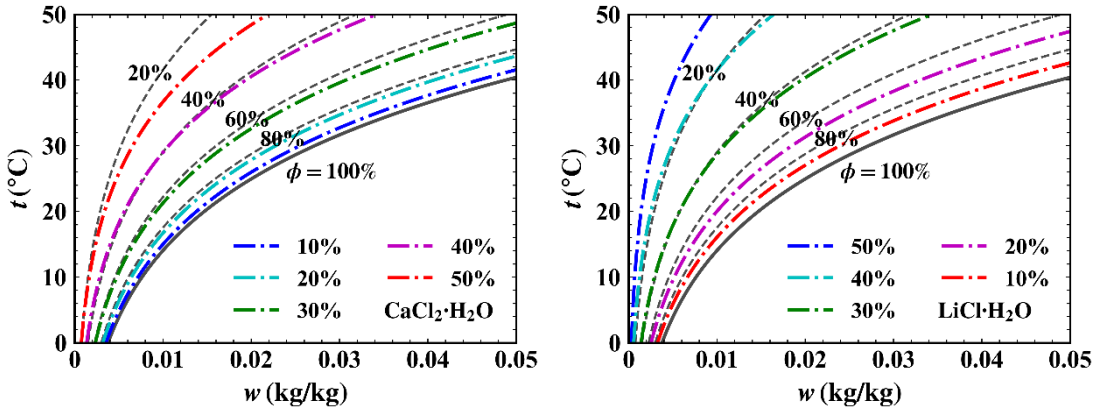

(a) $CaCl_2·H_2O$ (b) $LiCl·H_2O$

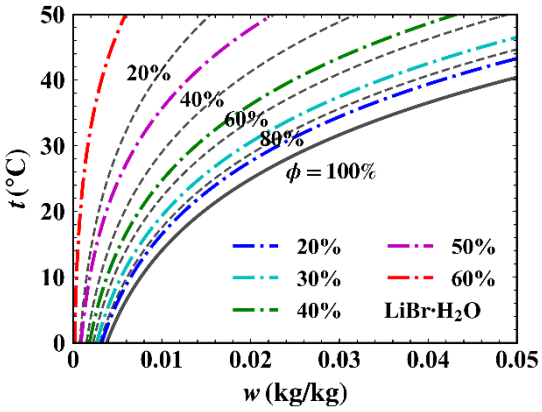

(c) LiBr·H₂O

Figure 5. States of **(a)** $CaCl_2 \cdot H_2O$, **(b)** $LiCl \cdot H_2O$, and **(c)** $LiBr \cdot H_2O$ solutions on the enthalpy-humidity chart.

At the same temperature, the density of solutions is higher than that of water, reducing drift losses and further minimizing water evaporation. Figure 6(a) shows the variation of solution density with temperature within the range of 0~40°C. Among the solutions at the same state on the enthalpy-humidity chart, $LiCl \cdot H_2O$ has the lowest density, $LiBr \cdot H_2O$ has a higher density, and $CaCl_2 \cdot H_2O$ has a density of approximately 1400 kg/m³. Furthermore, the density of these solutions is relatively insensitive to temperature changes. This stability is attributed to the strong intermolecular forces within the liquid phase, which maintain a consistent volume in the absence of phase transitions. The higher density of hygroscopic solutions compared to water enhances resistance to wind-induced carry-over, thereby effectively reducing drift losses in cooling towers.

Figure 6(b) shows the variation in specific enthalpy with temperature for solutions within the experimental range of 5 °C~40 °C. The specific enthalpy of the solutions increases with rising temperature. At the same temperature, $CaCl_2 \cdot H_2O$ exhibits the highest specific enthalpy, while $LiBr \cdot H_2O$ shows the lowest. Thus, at the same state, using $CaCl_2 \cdot H_2O$ as the cooling medium in cooling towers provides the maximum thermal efficiency.

In water-saving applications of cooling towers, the surface vapor pressure of the solution plays a critical role in determining water consumption. Figure 6(c) shows the variation in surface vapor pressure of the solutions with temperature, indicating an increase in surface vapor pressure with rising solution inlet temperature. Figure 6(d) illustrates the variation in surface vapor pressure with solution concentration, showing that higher concentrations result in lower surface vapor pressures.

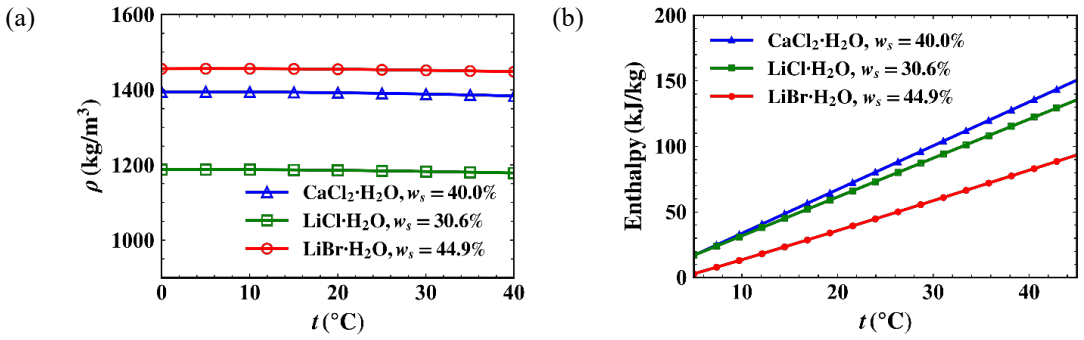

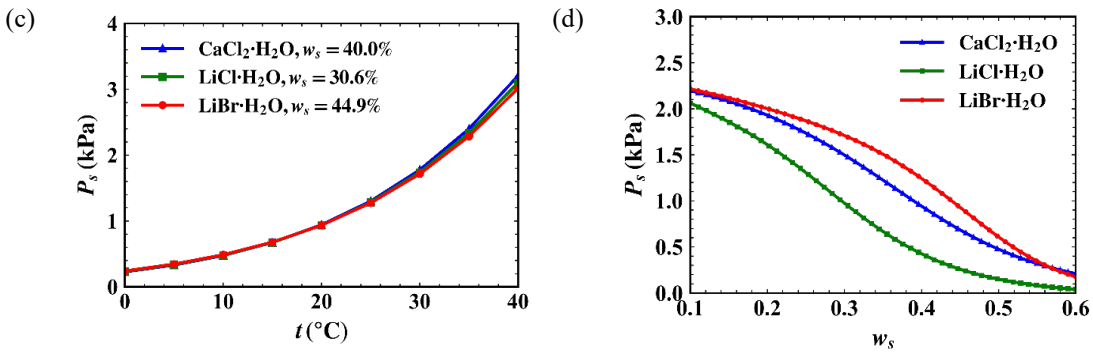

Figure 6. Properties of hygroscopic solutions. **(a)** Density, **(b)** specific enthalpy, and **(c)** surface vapor pressure versus temperature. **(d)** Surface vapor pressure versus concentration.

Using the 40 % $CaCl_2·H_2O$ solution as the cooling medium in the experimental cooling tower setup, the operational condition of a 20 °C solution inlet temperature is analyzed. On the enthalpy-humidity chart, solutions with the same state corresponding to $CaCl_2·H_2O$ at 20 °C and 40.0 % concentration are identified. These correspond to mass fractions of 44.9 % for $LiCl·H_2O$ and 30.6 % for $LiBr·H_2O$. Figure 7 illustrates the direct contact process between the solutions and moist air in the cooling tower system, calculated based on the experimental results of air and solution parameters. In this process, the solution cools along the constant relative humidity line (S1 → S2) while the air temperature rises (A1 → A2).

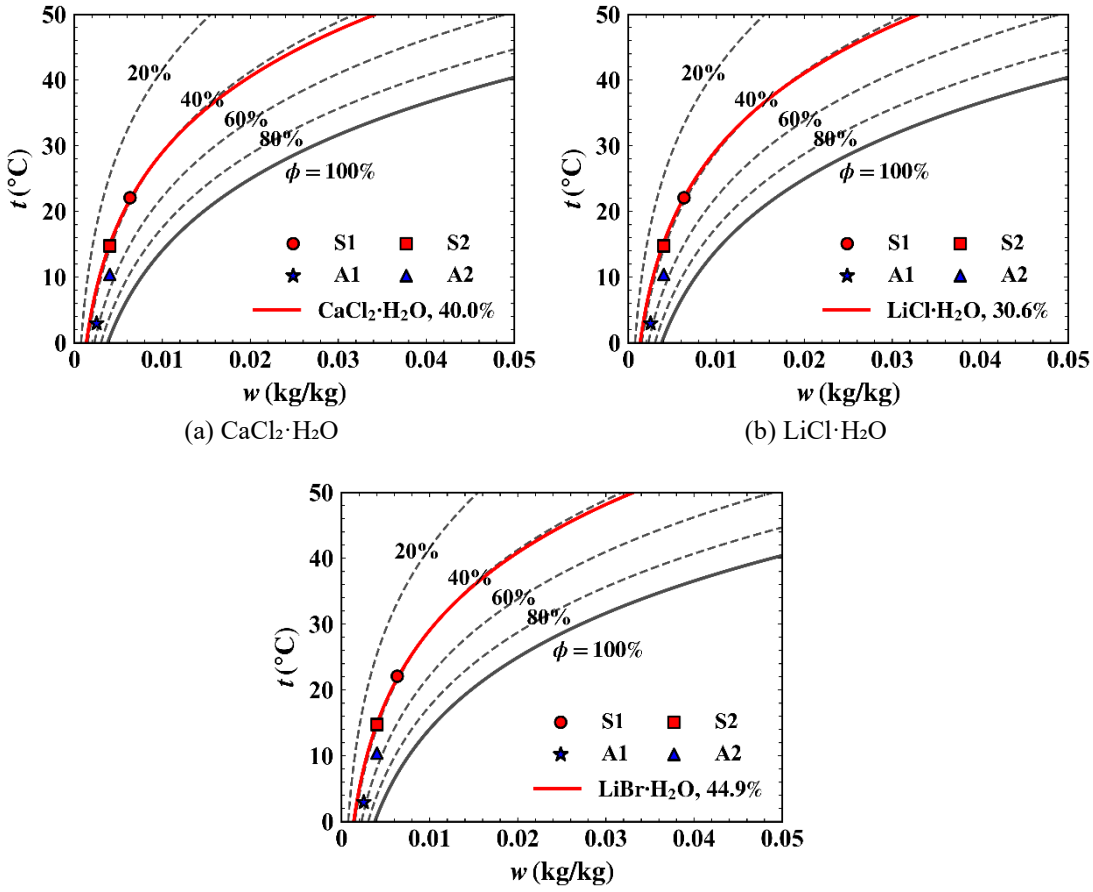

(a) $CaCl_2·H_2O$ (b) $LiCl·H_2O$

(c) $LiBr·H_2O$

Figure 7. Direct contact process between **(a)** $CaCl_2·H_2O$, **(b)** $LiCl·H_2O$, and **(c)** $LiBr·H_2O$ solutions and moist air in the cooling tower system.

4.2. Heat and mass transfer characteristics

This section presents a detailed analysis of the cooling tower's performance using the novel

hygroscopic solution as the cooling medium. The experiment uses $CaCl_2 \cdot H_2O$ hygroscopic solution as the cooling medium in the cooling tower. The analysis begins with the thermal efficiency of the cooling tower η. Figure 8(a) illustrates the cooling tower's thermal efficiency varying with inlet water temperature across different λ. The cooling tower demonstrates a thermal efficiency above 20% under most conditions, indicating good thermal performance. Additionally, thermal efficiency increases with inlet water temperature due to a larger temperature differential between water and air, enhancing convective heat transfer. Figure 8(b) depicts the thermal efficiency trend of the cooling tower as influenced by the λ. The thermal efficiency visibly improves with the λ across all inlet temperatures. A lower outlet water temperature under constant inlet and wet-bulb temperatures signifies higher cooling tower efficiency. Thus, a larger temperature difference in the cooling water correlates with efficiency improvements, given consistent inlet water temperature and flow rate. At an inlet temperature of 22 °C and an λ of 0.856, the peak thermal efficiency reaches 32.6 %. These results affirm that the new coolant maintains a good thermal efficiency.

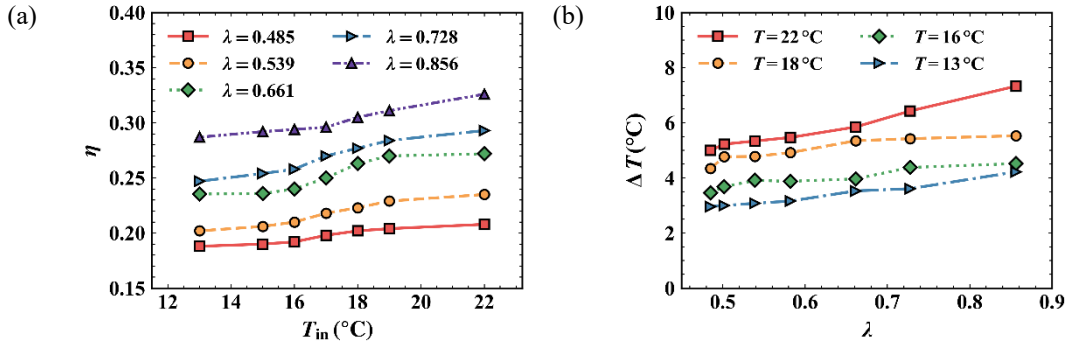

Figure 8. Cooling tower performance. **(a)** Thermal efficiency (η) versus inlet temperature (T_{in}) for various air-to-liquid ratios (λ). **(b)** Cooling range (ΔT) versus λ for various inlet temperatures.

Figure 9 shows how the cooling water range varies with the λ at different inlet water temperatures using new absorptive coolant. Generally, the cooling tower exhibits a relatively wide cooling water range. The cooling water range slightly increases with higher air-to-liquid ratios and significantly expands as the inlet water temperature rises. At an inlet temperature of 22 °C and the λ of 0.856, the cooling range extends up to 7.33 °C. This is mainly due to the increased λ enhancing solution-air contact efficiency per unit mass, reducing heat transfer resistance and boosting convective heat transfer.

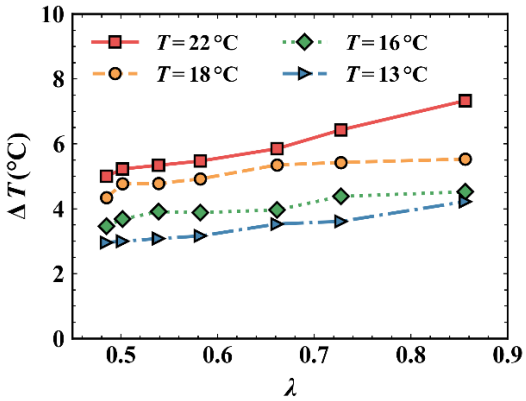

Figure 9. Variation in cooling range (ΔT) with λ for solution as the circulating medium, at different inlet temperatures.

To better evaluate the performance of the new cooling tower, the cooling number is introduced as a precise metric for assessing heat and mass transfer characteristics. Figure 10 shows the variation of the cooling number with λ under different inlet temperatures. The results indicate that the cooling capacity improves with both increasing inlet temperature and λ.

At an inlet temperature of 22°C, the cooling number reaches 0.43, 0.49, and 0.60 at λ values of 0.485, 0.661, and 0.856, respectively, demonstrating a nearly proportional relationship and reflecting effective transfer characteristics. This trend occurs because at lower λ, insufficient water leads to unsaturated

outlet air, water deficiency on the packing, and air short-circuiting—all reducing cooling effectiveness. As λ increases, cold air introduction becomes more efficient, allowing the outlet air to approach saturation. Beyond saturation, further increasing the water flow raises the outlet water temperature since the air reaches its heat absorption limit.

Thus, higher inlet temperatures and air-to-solution ratios further improve the cooling number in towers using hygroscopic solution. Although cooling efficiency increases with λ due to enhanced air-solution contact, a limit exists beyond which additional water only increases outlet temperature without improving cooling, as the air reaches its maximum heat absorption capacity.

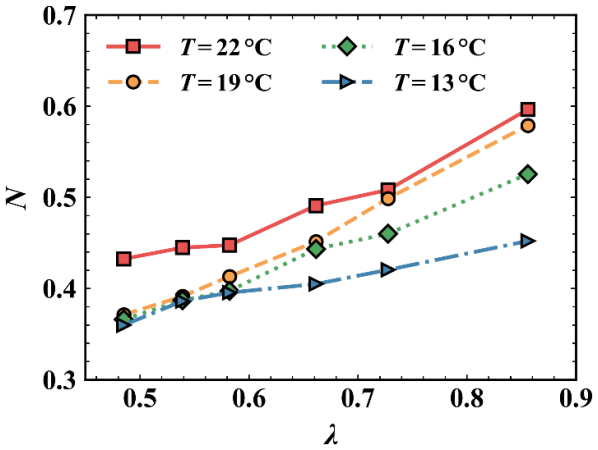

Figure 10. Under different inlet temperatures of the solution into the tower, the cooling number N varies with the λ.

The cooling efficiency in the tower increases with the λ due to better contact between the air and the solution. However, there's a limit to how much improving the flow rate can enhance cooling. When the λ is low, not enough water makes the air leave the tower too soon, lessening cooling efficiency. But as the λ increases, cooling becomes more effective until the air can't absorb more heat, marking a cooling limit. Beyond this point, adding more water only makes the outlet water warmer, as the air has reached its maximum cooling capacity. This shows there's a maximum effectiveness to cooling with cold air, beyond which no more heat can be absorbed.

Figure 11 displays the cooling performance parameters' variation for the novel absorptive solution cooling tower at an air-to-liquid ratio of 0.485. The parameters include cooling tower thermal efficiency (η), cooling water range (ΔT), and cooling number (N). With specific inlet air temperature, humidity, and λ, a higher inlet solution temperature expands the cooling range and boosts heat transfer capacity. As the inlet temperature increases from 12 °C to 22 °C, η, ΔT, and N change from 0.188 to 0.27, 2.95 to 5.0, and 0.38 to 0.434, respectively. This effect arises from the increased differential between water and ambient air wet-bulb temperatures as the inlet temperature rises, enhancing the heat transfer gradient and convective heat transfer rate. The trends of the three cooling performance parameters with respect to solution inlet temperature difference are consistent. Cooling performance improves with higher inlet temperatures, indicating the absorptive solution cooling tower aligns with traditional water-based cooling towers' performance patterns, without necessitating structural customization or modification.

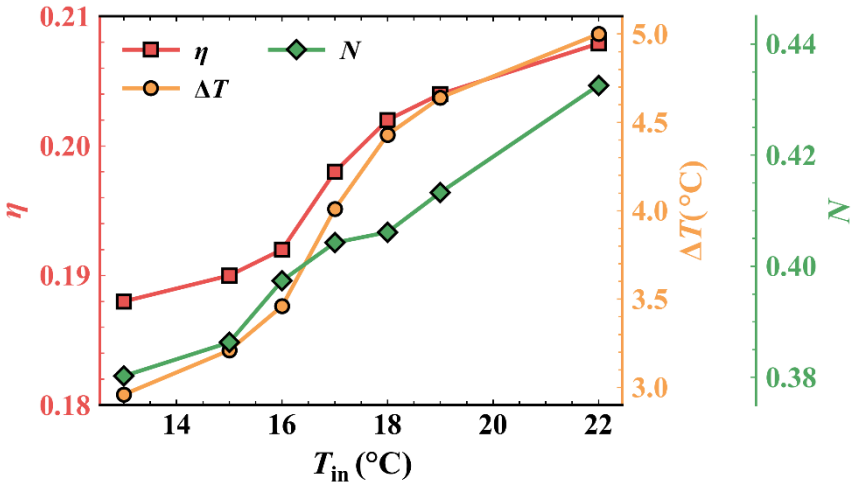

Figure 11 Cooling performance parameters (η, ΔT, and N) of the absorptive solution cooling tower as a function of solution inlet temperature.

4.3. Water consumption

Water usage in the cooling tower was precisely recorded via continuous monitoring of a water meter on the makeup water line. The water consumption study used two different inlet temperatures, 25 °C and 22 °C, with a flow rate of 30 m³/h. Figure 12 clearly demonstrates that cooling towers with a solution as the circulating fluid substantially reduce water consumption under the same conditions. Specifically, at an inlet temperature of 22 °C and after 600 minutes of operation, water consumption dropped from 1386 liters to 212 liters for the solution. This 84.72 % reduction in water usage showcases the solution's effectiveness in significantly reducing cooling tower water consumption.

The water-saving mechanisms in solution-based cooling towers are examined in this section. In these systems, the saturation vapor pressure of the cooling medium depends on both temperature and concentration, unlike traditional wet cooling towers. Since the saturation vapor pressure of pure water is higher than that of a solution, the liquid-phase composition can be altered by adding high-boiling-point, low-volatility solutes. When non-volatile, non-electrolyte solutes are dissolved into the solvent, some solute molecules occupy the solution surface, thereby reducing the number of solvent molecules that can evaporate per unit time compared to pure water. This mechanism is particularly effective in winter, where the use of salt solutions in wet cooling towers significantly reduces evaporation.

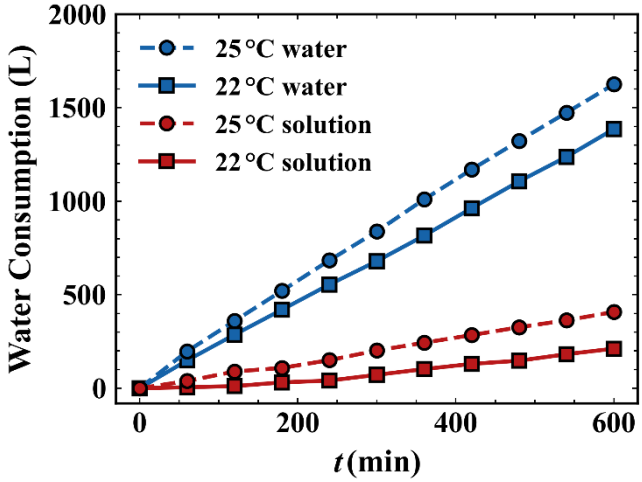

Figure 12. Variation in water consumption over time for solution cooling towers and traditional water cooling towers at inlet temperatures of 25 °C and 22 °C.

The key water-saving strategy in solution cooling towers lies in regulating the vapor pressure difference between the solution's surface and the moist air. By lowering this pressure difference, the mass

transfer driving force is reduced, which further decreases water consumption. The mass conservation and transfer relationship in hygroscopic solution cooling towers is expressed as:

$$dq_{ms} = dq_{ma} = \beta(P_s - P_a)dA, \quad (8)$$

where, q_{ms} and q_{ma} represents the solution and moist air flow rates (kg/s), respectively; β is the mass transfer coefficient (kg/(m²·Pa)); A is the tower's cross-sectional area (m²); and P_a and P_s are the vapor pressures of the solution and moist air (Pa), respectively. When $P_s = P_a$, resulting in $dq_{ms} = 0$, it indicates no evaporative losses, thus conserving water.

The main water-saving mechanism in hygroscopic solution cooling towers is regulating the hygroscopic liquid's surface vapor pressure, effectively reducing water evaporation. Fundamentally, the core strategy is to reduce the saturation vapor pressure at the phase interface. By dynamically adjusting temperature or concentration based on moist air's vapor pressure P_s, water evaporation rates can be controlled. Additionally, hygroscopic solutions absorb water from the air, aiding in water conservation.

Figure 13(a)-(c) shows the relationships among air temperature, surface vapor pressure, and the concentration of hygroscopic solutions ($CaCl_2 \cdot H_2O$, $LiCl \cdot H_2O$, and $LiBr \cdot H_2O$) under conditions of fixed solution bulk temperatures. The vapor pressure of moist air varies with changes in the dry-bulb and wet-bulb temperatures, and the solution's concentration adjusts to minimize mass transfer. When the vapor pressure differences between air and solution approach or exceed equilibrium, mass transfer ceases within the tower. By utilizing these properties, the average maximum and minimum air humidity levels over time can be used to select an optimal solution concentration that balances P_s and P_a. Furthermore, the water absorption ability of hygroscopic solutions compensates for some evaporation losses, maintaining a long-term moisture balance. Even with fluctuations in solution concentration, the time-averaged value remains constant, effectively minimizing evaporation losses. This behavior ensures sustained water conservation even under varying operating conditions.

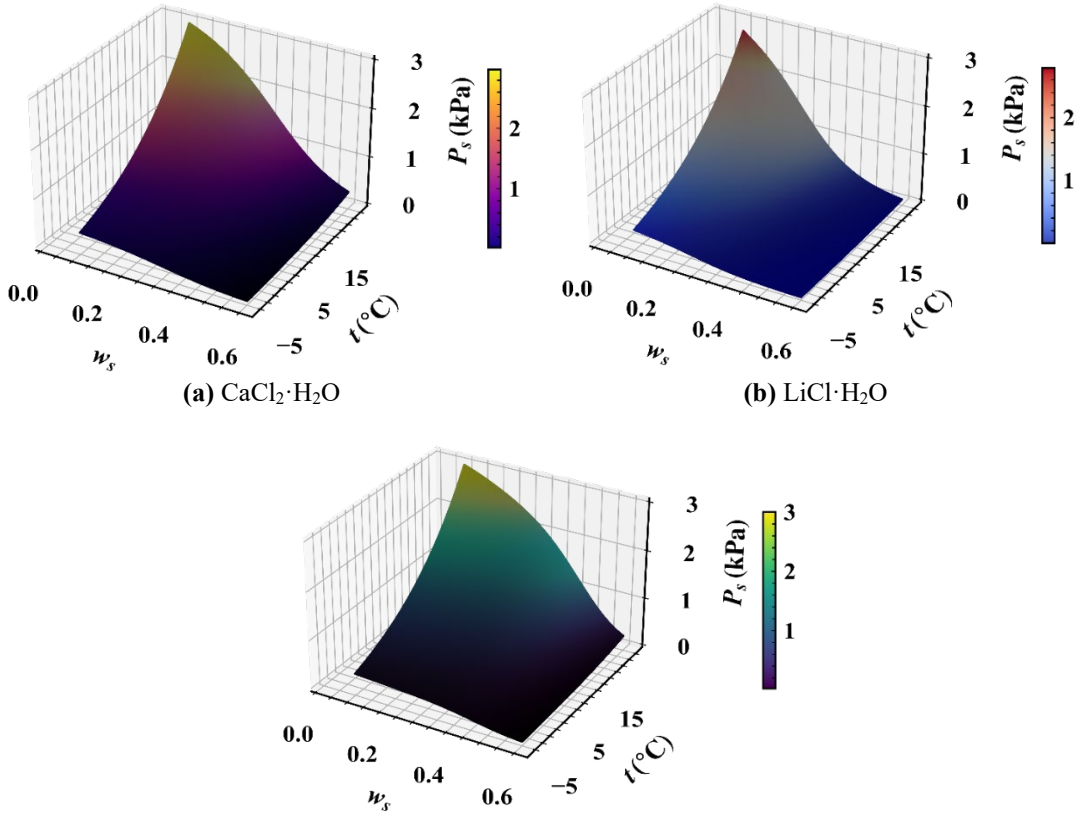

(a) $CaCl_2 \cdot H_2O$ **(b)** $LiCl \cdot H_2O$

(c) $LiBr \cdot H_2O$

Figure 13. Relationship between air bulk temperature and hygroscopic salt solution concentration under different surface vapor pressures.

Another water-saving factor is the reduction of blowdown losses. Blowdown losses in wet cooling towers arise from the accumulation of low-solubility salts in the circulating water. Continuous water evaporation increases salt concentration, causing corrosion and scaling on heat exchange surfaces and worsening heat transfer conditions. Conversely, solution cooling towers neutralize evaporative

concentration through periodic absorption and dilution, virtually eliminating evaporative losses. The absorbed water comes from the air, reducing the need for frequent blowdowns beyond removing airborne dust, thus effectively cutting blowdown losses. Additionally, as discussed in the density analysis in Section 4.1, the higher density of hygroscopic solutions (1.1 to 1.5 times that of water) in cooling towers significantly reduces susceptibility to wind-induced carry-over, thereby minimizing drift losses.

Figure 14 illustrates a comparison between the water-saving rate achieved by the solution-based wet cooling tower introduced in this study and those reported in existing literature on water-saving cooling towers. Our study achieved a water-saving rate of 84.72 %, surpassing nearly all reported rates in current research on enhancing wet cooling tower efficiency (Askari et al., 2016, Shublaq and Sleiti, 2020, Lee et al., 2020, Liu et al., 2023, Wan et al., 2020, Deng et al., 2022, Yu et al., 2021, Deziani et al., 2017, Sadafi et al., 2015, García Cutillas et al., 2017).

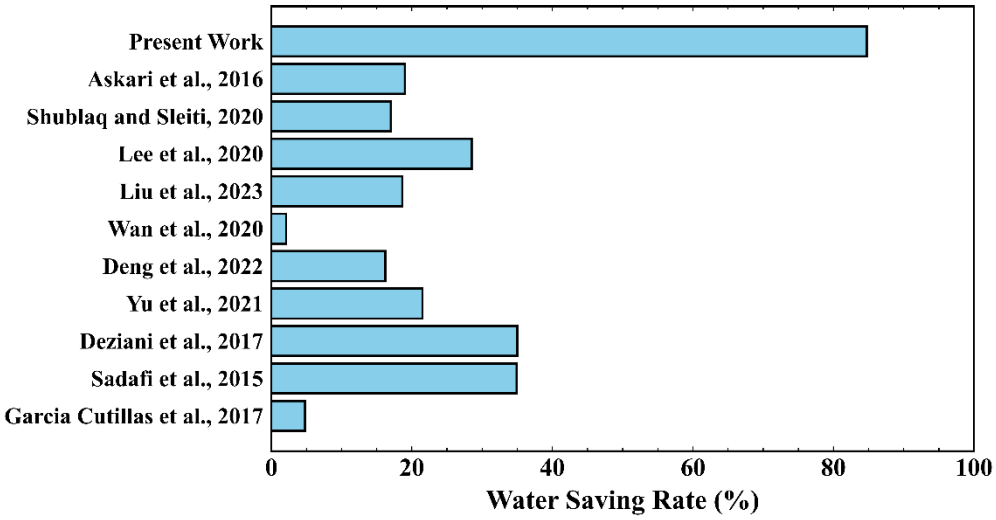

Figure 14. Comparison of water consumption with the literature values.

For a more detailed and direct quantitative comparison, the results are summarized and ranked in Table 2. The table clearly shows that the performance of our solution-based cooling tower represents a substantial advancement in the field. While previous leading studies reported water-saving rates of up to 35% (Deziani et al., 2017) and 34.9% (Sadafi et al., 2015), our achieved rate of 84.72% is more than double the next highest value, underscoring the novelty and significance of this work.

Table 2. Comparison of reported water saving rates in representative studies.

Rank	Study	Year	Water Saving Rate (%)
1	Present Work	—	84.72
2	Deziani et al.	2017	35
3	Sadafi et al.	2015	34.9
4	Lee et al.	2020	28.5
5	Yu et al.	2021	21.5
6	Askari et al.	2016	19
7	Liu et al.	2023	18.62
8	Shublaq and Sleiti	2020	17
9	Deng et al.	2022	16.2
10	Garcia Cutillas et al.	2017	4.8
11	Wan et al.	2020	2.11

Moreover, hygroscopic solutions, which are mixtures of water and solutes, generally have lower crystallization temperatures compared to pure water. While the freezing point of water is 0°C under standard atmospheric pressure, the crystallization points of hygroscopic solutions are typically below 0 °C. For instance, based on the crystallization curves of $CaCl_2 \cdot H_2O$ solutions calculated by Conde (Conde, 2004) solutions with concentrations ranging from 21.6 % to 34.5 % remain uncrystallized at -20 °C, and those with concentrations between 25.1 % and 33.0 % do not crystallize even at -30 °C. Due to their lower crystallization temperatures, hygroscopic solutions exhibit superior anti-freezing performance in wet cooling towers compared to water, offering significant advantages in cold climates.

4.4. Stability and economic viability analysis

The long-term stability of the hygroscopic solution is critical for its practical application and is supported by a combination of inherent thermodynamic mechanisms and straightforward operational measures. The system's fundamental stability stems from its ability to actively manage the vapor pressure difference between the solution and ambient air by dynamically adjusting solution temperature or concentration (as illustrated in Figure 13). Experimental observations suggest that even with minor fluctuations, the time-averaged solution concentration remains stable under consistent operating conditions, effectively minimizing net evaporative losses. This stability is further reinforced by the intrinsic hygroscopic nature of the solutions, which enables them to absorb water vapor from the air, thereby compensating for potential residual evaporative losses. This internal water-balancing mechanism is crucial for maintaining a stable solution concentration and volume over extended periods.

Operationally, this inherent stability is supported by simple monitoring protocols. Water consumption is continuously tracked, and solution density is periodically measured to confirm concentration stability. An automatic replenishment system, connected via a float valve, maintains the liquid level in the cooling tower, while routine inspections of the packing material and other wetted components ensure system integrity. This synergy between the solution's intrinsic properties and a simple maintenance regimen helps ensure that the thermophysical properties and cooling performance remain stable during long-term operation. Furthermore, the system's chemical stability appears to be enhanced. Unlike traditional wet cooling towers that require frequent blowdown due to the accumulation of dissolved solids, the solution-based system mitigates evaporative concentration through periodic moisture absorption. This process significantly lowers the required volume and frequency of discharges, thereby reducing the buildup of impurities that can lead to scaling. To further assess the material compatibility for long-term use, electrochemical tests were conducted on stainless steel, a common material in cooling system components. The results revealed corrosion current densities in the order of 10^{-8} to 10^{-9} A/cm², a rate consistent with levels generally considered negligible in engineering contexts. Finally, the superior antifreeze properties of the hygroscopic solutions contribute significantly to operational stability in cold climates by eliminating freezing-related downtime and maintenance.

The discussion of long-term stability naturally extends to the environmental sustainability of the solution's lifecycle. An assessment of sustainability should consider the transportation, storage, and disposal of the hygroscopic salts used, such as calcium chloride. These salts are industrially common chemicals with low toxicity and are non-volatile, which facilitates their transportation and storage protocols. The significantly reduced need for blowdown discharge also minimizes the volume of waste generated during operation. In the event of system decommissioning or solution replacement, the disposal of these saline solutions can be accommodated by established industrial wastewater treatment protocols for brine.

Beyond this, the economic implications of utilizing hygroscopic solution-based cooling towers are also highly significant. To assess the economic viability, a cost-benefit analysis was conducted based on a case study of a data center park in Beijing with a 10 MW IT power design and a 15,000 kW total cooling load. The analysis assumes the data center's cooling system operates continuously throughout the year, with an average IT equipment load factor (η_{IT}) of 70%.

The primary economic benefit stems from the drastic reduction in water consumption. The annual water usage is quantified using the Water Usage Effectiveness (WUE) metric. The annual water saving (G_{water}) can be calculated with the following equation:

$$G_{\mathrm{water}} = \eta_{\mathrm{IT}} W_{\mathrm{IT}} WUE, \tag{9}$$

where W_{IT} represents the total annual energy consumed by the IT equipment. For a conventional water-based cooling tower, a typical WUE of 2.00 L/(kW·h) is assumed. In contrast, the proposed solution-based system, after accounting for thermal efficiency and other engineering redundancies, achieves a WUE of 0.48 L/(kW·h). This difference results in an annual reduction in makeup water of 93,206.4 tons. Based on Beijing's current non-residential water price of CNY 9.52 per ton (USD 1.32 per ton), this translates directly to an annual cost saving of approximately USD 123,200.

The implementation of this technology introduces an initial investment and ongoing operational costs. The principal incremental initial investment is the one-time procurement of the hygroscopic solute. At a market price of approximately USD 0.625/kg, the initial filling cost for the system is estimated to be USD 81,300. The annual operational expenditures, primarily for minor solution replenishment and system maintenance, are estimated at USD 1,670. It is assumed that other operational costs, such as those related to electricity for pumps and general maintenance, are comparable between the two systems, as the increased pumping energy for the denser solution is offset by savings from the water makeup and treatment systems, and the need for winter anti-freezing measures in traditional systems is eliminated.

The annual net saving (S_{net}) is therefore determined by subtracting the annual operational expenses (C_o) from the annual water cost savings (S_{water}), resulting in approximately USD 121,500. The

investment payback period (n) can then be calculated by dividing the initial investment cost (C_i) by the annual net saving:

$$n = \frac{C_i}{S_{net}}, \tag{10}$$

where C_i is the initial investment cost (USD 81,300) and S_{net} is the annual net saving (USD 121,500). Based on this calculation, the investment payback period is approximately 0.7 years. This rapid return on investment demonstrates the significant economic advantages of the proposed technology, greatly enhancing its adaptability in water-scarce regions or areas with high water tariffs and providing an effective technological pathway for the green development of data centers.

To provide a holistic summary and directly contrast the proposed technology with conventional methods, a comparative analysis is presented. Table 3 offers a detailed, side-by-side breakdown of the key performance, operational, and economic metrics discussed throughout this study. The table quantifies the substantial improvements in water-saving rate, antifreeze capability, and economic viability, while noting the comparable thermal performance.

Table 3. Comparative Summary of Cooling Tower Technologies.

Feature / Metric	Traditional water-based cooling tower	Proposed solution-based system
Primary Cooling Medium	Water	Hygroscopic solution
Water-Saving Rate	Baseline	Up to 84.72%
Thermal Performance	High	Slightly lower
Antifreeze Capability	Poor (freezes at 0°C and requires winter freeze protection)	Excellent (crystallization point <. -30°C)
Blowdown Requirement	Frequent (to control dissolved solids)	Significantly reduced (primarily for dust removal)
Initial Investment	Baseline	Incremental cost for initial solute fill (approx. USD 81,300 in case study)
Economic Viability	——	~ 0.7 years (case study result)
Environmental Impact	High water withdrawal	Greatly reduced water footprint

To synthesize the metrics from Table 3 into a single, intuitive comparison, a comparative radar chart is presented in Figure 15. The chart plots the performance of each system across six key dimensions. As is immediately apparent from the graphic, the proposed system exhibits a significantly larger and more well-rounded performance profile, demonstrating clear superiority across most metrics. In contrast, the traditional system's profile is substantially smaller. This stark visual contrast provides an intuitive confirmation of the overall superiority and practical value of the hygroscopic solution-based cooling technology.

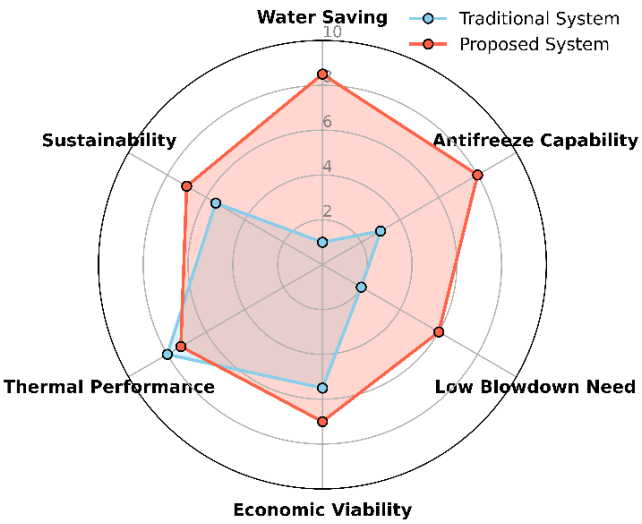

Figure 15. Comparative performance summary of the traditional and proposed cooling systems across key metrics.

5. Conclusion

This study presents a novel water-saving counterflow wet cooling tower that uses desiccant solutions as an economical, efficient, non-toxic, and non-corrosive cooling medium to replace traditional water. The application of common hygroscopic salt solutions—$CaCl_2 \cdot H_2O$, $LiBr \cdot H_2O$, and $LiCl \cdot H_2O$—was analyzed through heat and mass transfer studies. Mathematical models were employed to calculate surface vapor pressure, density, and specific enthalpy. Enthalpy-humidity charts identified equivalent states for $CaCl_2 \cdot H_2O$ at 20 °C and 40.0 % concentration, corresponding to 44.9 % for $LiCl \cdot H_2O$ and 30.6 % for $LiBr \cdot H_2O$. Specific enthalpy increased with temperature, with $CaCl_2 \cdot H_2O$ exhibiting the highest values, making it the most efficient cooling medium.

A mechanically ventilated counterflow experimental system was developed to evaluate water-saving and cooling performance. Experimental results showed that cooling capacity improved with higher inlet temperatures and increasing air-to-solution ratios (λ). At an inlet temperature of 22 °C and λ values of 0.485, 0.661, and 0.856, the cooling numbers were 0.43, 0.49, and 0.60, respectively, indicating a proportional relationship with λ. As the inlet temperature increased from 12 °C to 22 °C, thermal efficiency (η), temperature range (ΔT), and cooling number (N) increased from 0.188 to 0.27, 2.95 °C to 5.0 °C, and 0.38 to 0.434, respectively, highlighting the system's efficient heat transfer characteristics.

The experimental results revealed that hygroscopic salt solutions reduced water consumption by up to 84.72 % compared to traditional water-based systems—the highest reduction reported to date. The higher density of these solutions (1.1–1.5 times that of water) minimized drift losses, while less frequent blowdown further reduced discharge losses. Additionally, $CaCl_2$ solutions with concentrations of 25.1 %–33.0 % remained uncrystallized even at -30 °C, demonstrating excellent anti-freezing capabilities and significant advantages in cold climates. These insights underline the potential for reducing water consumption in data center cooling systems and integrating sustainable practices into environmentally friendly infrastructure.

Acknowledgements

The authors gratefully acknowledge financial support from the Tsinghua University China Mobile Communication Group Co., Ltd. Joint Research Institute Project (20232930009), and the Collaborative Key Projects with Academicians of Hebei Tsinghua Development Research Institute (225A9912D).

References

Abbas, A. M., Huzayyin, A. S., Mouneer, T. A. & Nada, S. A. 2021. Thermal management and performance enhancement of data centers architectures using aligned/staggered in-row cooling arrangements. *Case Studies in Thermal Engineering,* 24**,** 100884. https://doi.org/10.1016/j.csite.2021.100884

Akbarpour Ghazani, M., Hashem-ol-Hosseini, A. & Emami, M. D. 2017. A comprehensive analysis of a

laboratory scale counter flow wet cooling tower using the first and the second laws of thermodynamics. *Applied Thermal Engineering,* 125**,** 1389-1401. https://doi.org/10.1016/j.applthermaleng.2017.07.090

Askari, S., Lotfi, R., Seifkordi, A., Rashidi, A. M. & Koolivand, H. 2016. A novel approach for energy and water conservation in wet cooling towers by using MWNTs and nanoporous graphene nanofluids. *Energy Conversion and Management,* 109**,** 10-18. https://doi.org/10.1016/j.enconman.2015.11.053

Asvapoositkul, W. & Kuansathan, M. 2014. Comparative evaluation of hybrid (dry/wet) cooling tower performance. *Applied Thermal Engineering,* 71**,** 83-93. https://doi.org/10.1016/j.applthermaleng.2014.06.023

Chaudhari, S. & Patil, K. 2002. Thermodynamic properties of aqueous solutions of lithium chloride. *Physics and Chemistry of Liquids,* 40**,** 317-325. https://doi.org/10.1080/0031910021000004883

Cheung, H. & Wang, S. 2019. Optimal design of data center cooling systems concerning multi-chiller system configuration and component selection for energy-efficient operation and maximized free-cooling. *Renewable Energy,* 143**,** 1717-1731. https://doi.org/10.1016/j.renene.2019.05.127

Conde, M. R. 2004. Properties of aqueous solutions of lithium and calcium chlorides: formulations for use in air conditioning equipment design. *International Journal of Thermal Sciences,* 43**,** 367-382. https://doi.org/10.1016/j.ijthermalsci.2003.09.003

Cuce, P. 2025. Evaporative Cooling Technologies: From Past to Present. *Journal of Global Decarbonisation***,** 1-40. 10.17184/eac.9493

Deng, W. & Sun, F. 2024. Performance analysis and multi-objective optimization of mechanical draft wet cooling towers based on water saving, plume and cooling characteristics. *International Journal of Thermal Sciences,* 196**,** 108656. https://doi.org/10.1016/j.ijthermalsci.2023.108656

Deng, W., Sun, F., Chen, K. & Zhang, X. 2022. The research on plume abatement and water saving of mechanical draft wet cooling tower based on the rectangle module. *International Communications in Heat and Mass Transfer,* 136**,** 106184. https://doi.org/10.1016/j.icheatmasstransfer.2022.106184

Deziani, M., Rahmani, K., Roudaki, S. M. & Kordloo, M. 2017. Feasibility study for reduce water evaporative loss in a power plant cooling tower by using air to Air heat exchanger with auxiliary Fan. *Desalination,* 406**,** 119-124. https://doi.org/10.1016/j.desal.2015.12.007

Du, S., Cui, Z., Wang, R. Z., Wang, H. & Pan, Q. 2024. Development and experimental study of a compact silica gel-water adsorption chiller for waste heat driven cooling in data centers. *Energy Conversion and Management,* 300**,** 117985. https://doi.org/10.1016/j.enconman.2023.117985

El-Dessouky, H. T. A., Al-Haddad, A. & Al-Juwayhel, F. 1997. A Modified Analysis of Counter Flow Wet Cooling Towers. *Journal of Heat Transfer,* 119**,** 617-626. https://doi.org/10.1115/1.2824150

El Marazgioui, S. & El Fadar, A. 2022. Impact of cooling tower technology on performance and cost-effectiveness of CSP plants. *Energy Conversion and Management,* 258**,** 115448. https://doi.org/10.1016/j.enconman.2022.115448

García Cutillas, C., Ruiz Ramírez, J. & Lucas Miralles, M. 2017. Optimum Design and Operation of an HVAC Cooling Tower for Energy and Water Conservation. *Energies,* 10. https://doi.org/10.3390/en10030299

Han, Z., Xue, D., Wei, H., Ji, Q., Sun, X. & Li, X. 2021. Study on operation strategy of evaporative cooling composite air conditioning system in data center. *Renewable Energy,* 177**,** 1147-1160. https://doi.org/10.1016/j.renene.2021.06.046

He, W., Zhang, J., Li, H., Liu, S., Wang, Y., Lv, B. & Wei, J. 2022. Optimal thermal management of server cooling system based cooling tower under different ambient temperatures. *Applied Thermal Engineering,* 207**,** 118176. https://doi.org/10.1016/j.applthermaleng.2022.118176

Hill, G. B., Pring, E. & Osborn, P. D. 2013. *Cooling towers: principles and practice*, Butterworth-Heinemann.

Imani-Mofrad, P., Zeinali Heris, S. & Shanbedi, M. 2018. Experimental investigation of the effect of different nanofluids on the thermal performance of a wet cooling tower using a new method for equalization of ambient conditions. *Energy Conversion and Management,* 158**,** 23-35. https://doi.org/10.1016/j.enconman.2017.12.056

Javadpour, R., Zeinali Heris, S. & Mohammadfam, Y. 2021. Optimizing the effect of concentration and flow rate of water/ MWCNTs nanofluid on the performance of a forced draft cross-flow cooling tower. *Energy,* 217**,** 119420. https://doi.org/10.1016/j.energy.2020.119420

Khamis Mansour, M. 2017. On the Merkel Equation: Novel ε-Number of Transfer Unit Correlations for Indirect Evaporative Cooler Under Different Lewis Numbers. *Journal of Thermal Science and Engineering Applications,* 9. https://doi.org/10.1115/1.4036204

Kutlu, C., Erdinç, M., Ehtiwesh, A., Bottarelli, M., Su, Y. & Riffat, S. 2025. Evaluation of operation

control parameters of a residential solar organic Rankine cycle with effects of expander-generator coupling. *Journal of Global Decarbonisation*, 1-19. 10.17184/eac.9437
Lee, B., Roh, C. W., Choi, B. S., Wang, E., Ra, H.-S., Cho, J., Cho, J., Shin, H., Choi, J. W. & Lee, G. 2020. Experimental evaluations on the outdoor air-based methods for water saving and plume abatement of cooling tower. *International Journal of Low-Carbon Technologies,* 15, 421-426. https://doi.org/10.1093/ijlct/ctz078
Li, G., Sun, Z., Wang, Q., Wang, S., Huang, K., Zhao, N., Di, Y., Zhao, X. & Zhu, Z. 2023. China's green data center development: Policies and carbon reduction technology path. *Environmental Research*, 116248. https://doi.org/10.1016/j.envres.2023.116248
Liu, L., Xi, Y., Zhang, L., Yu, Z., Sun, C., Yang, L., Zhang, Z., Zhou, C., Dong, K. & Liu, K. 2023. Research on water saving performance of a new type of demisting cooler for cooling towers. *Chemical Engineering and Processing - Process Intensification,* 192, 109488. https://doi.org/10.1016/j.cep.2023.109488
Masanet, E., Shehabi, A., Lei, N., Smith, S. & Koomey, J. 2020. Recalibrating global data center energy-use estimates. *Science,* 367, 984-986. https://doi.org/10.1126/science.aba3758
Merkel, F. 1925. Verdunstungskühlung. *(No Title)*.
Mirabdolah Lavasani, A., Namdar Baboli, Z., Zamanizadeh, M. & Zareh, M. 2014. Experimental study on the thermal performance of mechanical cooling tower with rotational splash type packing. *Energy Conversion and Management,* 87, 530-538. https://doi.org/10.1016/j.enconman.2014.07.036
Ni, J. & Bai, X. 2017. A review of air conditioning energy performance in data centers. *Renewable and sustainable energy reviews,* 67, 625-640. https://doi.org/10.1016/j.rser.2016.09.050
Pátek, J. & Klomfar, J. 2006. A computationally effective formulation of the thermodynamic properties of LiBr–H2O solutions from 273 to 500K over full composition range. *International Journal of Refrigeration,* 29, 566-578. https://doi.org/10.1016/j.ijrefrig.2005.10.007
Qi, X., Liu, Y., Guo, Q., Yu, J. & Yu, S. 2016. Performance prediction of seawater shower cooling towers. *Energy,* 97, 435-443. https://doi.org/10.1016/j.energy.2015.12.125
Qu, X., Guo, Q., Qi, X. & Yu, Y. 2024. Numerical and experimental study on performance of seawater cooling towers based on a comprehensive coupling model. *Applied Thermal Engineering,* 236, 121583. https://doi.org/10.1016/j.applthermaleng.2023.121583
Refrigeration, C. A. o. (ed.) 2023. *Annual Development Research Report on Chinese Data Center Cooling Technology 2022*.
Sadafi, M. H., Jahn, I., Stilgoe, A. B. & Hooman, K. 2015. A theoretical model with experimental verification for heat and mass transfer of saline water droplets. *International Journal of Heat and Mass Transfer,* 81, 1-9. https://doi.org/10.1016/j.ijheatmasstransfer.2014.10.005
Sharqawy, M. H., Lienhard, J. H. & Zubair, S. M. 2011. On thermal performance of seawater cooling towers. https://doi.org/10.1115/IHTC14-23200
Shublaq, M. & Sleiti, A. K. 2020. Experimental analysis of water evaporation losses in cooling towers using filters. *Applied Thermal Engineering,* 175. https://doi.org/10.1016/j.applthermaleng.2020.115418
Siddig-Mohammed, B., Watson, F. & Holland, F. A. 1983. Study of the operating characteristics of a reversed absorption heat pump system (heat transformer). *Chemical engineering research and design,* 61, 283-289.
Silva-Llanca, L., Ponce, C., Bermúdez, E., Martínez, D., Díaz, A. J. & Aguirre, F. 2023. Improving energy and water consumption of a data center via air free-cooling economization: The effect weather on its performance. *Energy Conversion and Management,* 292, 117344. https://doi.org/10.1016/j.enconman.2023.117344
Suman, S., Calautit, J. K., Wei, S., Tien, P., Chen, X., Wang, Z. & Sun, H. 2025. Assessing the Energy-Saving Potential of Passive Strategies in Commercial Buildings in the Top Upcoming Megacities. 1, 1-21. 10.61552/EC.2025.001
Taghian Dehaghani, S. & Ahmadikia, H. 2017. Retrofit of a wet cooling tower in order to reduce water and fan power consumption using a wet/dry approach. *Applied Thermal Engineering,* 125, 1002-1014. https://doi.org/10.1016/j.applthermaleng.2017.07.069
Wan, D., Gao, S., Liu, M., Li, S. & Zhao, Y. 2020. Effect of cooling water salinity on the cooling performance of natural draft wet cooling tower. *International Journal of Heat and Mass Transfer,* 161, 120257. https://doi.org/10.1016/j.ijheatmasstransfer.2020.120257
Whitman, W. G. 1962. The two film theory of gas absorption. *International Journal of Heat and Mass Transfer,* 5, 429-433. https://doi.org/10.1016/0017-9310(62)90032-7
Xi, Y., Yu, Z., Zhang, L., Yu, A., Liu, L., Bao, B., Zhao, Y., Zhou, C., Wu, B. & Dong, K. 2023. Research on heat and mass transfer characteristics of a counterflow wet cooling tower using a new type

of straight wave packing. *International Journal of Thermal Sciences,* 193**,** 108540. https://doi.org/10.1016/j.ijthermalsci.2023.108540

Xu, S., Zhang, H. & Wang, Z. 2023. Thermal Management and Energy Consumption in Air, Liquid, and Free Cooling Systems for Data Centers: A Review. *Energies,* 16. https://doi.org/10.3390/en16031279

Yan, W., Cui, X., Meng, X., Yang, C., Zhang, Y., Liu, Y., An, H. & Jin, L. 2024. Multi-objective optimization of hollow fiber membrane-based water cooler for enhanced cooling performance and energy efficiency. *Renewable Energy,* 222**,** 119892. https://doi.org/10.1016/j.renene.2023.119892

Yu, Z., Sun, C., Zhang, L., Bao, B., Li, Y., Bu, S. & Xu, W. 2021. Analysis of a novel combined heat exchange strategy applied for cooling towers. *International Journal of Heat and Mass Transfer,* 169**,** 120910. https://doi.org/10.1016/j.ijheatmasstransfer.2021.120910

Yuan, W., Sun, F., Liu, R., Chen, X. & Li, Y. 2020. The Effect of Air Parameters on the Evaporation Loss in a Natural Draft Counter-Flow Wet Cooling Tower. *Energies,* 13. https://doi.org/10.3390/en13236174

Zhang, P., Li, K., Liu, Q., Zou, Q., Liang, R., Qin, L. & Wang, Y. 2024. Thermal stratification characteristics and cooling water shortage risks for pumped storage reservoir–green data centers under extreme climates. *Renewable Energy,* 229**,** 120697. https://doi.org/10.1016/j.renene.2024.120697

Zhao, Z., Gao, J., Zhu, X. & Qiu, Q. 2023. Experimental study of the corrugated structure of film packing on thermal and resistance characteristics of cross-flow cooling tower. *International Communications in Heat and Mass Transfer,* 141**,** 106610. https://doi.org/10.1016/j.icheatmasstransfer.2022.106610